

## **Infrared Laser Ablation of Poly(vinylidene fluoride): The Loss of HF**

Petr N. Grakovich,<sup>a,b</sup> Sadulla R. Allayarov,<sup>a</sup> Matthew P. Confer,<sup>c</sup> Leonid A. Kalinin,<sup>b</sup> Ivan A. Frolov,<sup>a</sup> Tatyana N. Rudneva,<sup>a</sup> Leonid F. Ivanov,<sup>b</sup> and David A. Dixon<sup>c,\*</sup>

<sup>a</sup> Institute of Problems of Chemical Physics of the Russian Academy of Sciences,  
Chernogolovka, the Moscow Region, 142432, Russia

<sup>b</sup> V. A. Belyi Metal-Polymer Research Institute, National Academy of Sciences of Belarus,  
Gomel 246050, Belarus

<sup>c</sup> Department of Chemistry and Biochemistry, The University of Alabama, Shelby Hall, Box  
870336, Tuscaloosa, AL, USA

\* Corresponding author. E-mail address: [dadixon@bama.ua.edu](mailto:dadixon@bama.ua.edu) (D.A. Dixon).

### **Abstract**

The mechanism and kinetics of infrared laser ablation of poly(vinylidene fluoride) (PVDF) in vacuum have been investigated to understand how this can be used as a polymer processing technology. The laser heats the surface and initiates decomposition of macromolecules in the molten polymer layer which rapidly leads to production of an ablative flow of polymer decomposition products. There is only a short induction period of up to 2 s before ablation begins. After the initial period, the rate of mass loss increases linearly with the time of laser exposure. Spherical particles with an average diameter of about 100 nm are formed on the surface of the powder coating obtained by laser ablation. The particle distribution ranges from 50 nm to 300 nm. The main gaseous product of ablation is HF from dehydrofluorination. A second important ablation process is the formation of gaseous carbenes generated during secondary

reactions. Proposed ablation reactions due to laser-induced thermal dehydrofluorination occur in two stages. In the first stage, a double bond appears in PVDF due to direct loss of HF. Subsequent detachment of HF leads to the appearance of both triple bonds and cumulene bonds.

Key words: poly(vinylidene fluoride), IR laser ablation, mechanism, kinetics, products, FTIR spectroscopy, supramolecular structure.

## 1. Introduction

Poly(vinylidene fluoride) has high strength, hardness (Brinell hardness up to 90 MPa), high elasticity, abrasion resistance, solubility in aprotic solvents and easy processability and has a number of technological applications [1,2,3,4]. PVDF is known for its electroactive properties, non-linear optical susceptibility, and an unusually high dielectric constant for a polymer [5]. There are five chain conformations in semicrystalline PVDF:  $\alpha$ ,  $\beta$ ,  $\gamma$ ,  $\alpha\beta$ , and  $\varepsilon$  [6,7] with only the  $\beta$  conformation having the piezoelectric and pyroelectric properties. These electroactive properties of the PVDF depend on the phase content, microstructure, and degree of crystallinity of the material, all of which depend on the processing conditions [8,9]. An important difference between PVDF and other fluoropolymers is its high resistance to UV light and ionizing  $\gamma$ -radiation [10,11], so there is significant interest in using PVDF for nuclear and aerospace engineering technologies. For the successful application of PVDF in such technologies in the presence of potential irradiation sources, the behavior and properties of the polymer under irradiation need to be known. The main process occurring on irradiation of PVDF by high energy radiation sources including fast electrons [12,13,14],  $\gamma$ -radiation [15,16], X-rays [17,18], energetic ions [19,20,21], protons [22,23,24] and high-power lasers, [25,26,27,28] is dehydrofluorination [29] leading to the formation of small amounts of unsaturated and partially fluorinated structures. The main carbon chain of PVDF does not undergo destructive degradation, unlike the radiolysis of perfluorinated polymers [4,10,11]. The reason for the effective release of hydrogen fluoride during radiolysis of PVDF is the uniform distribution of hydrogen and fluorine atoms along the chain. This decomposition feature of PVDF is also observed in its pyrolysis.

High-energy radiation has a significant effect on the molecular topological structure of PVDF [30], so it can be used to increase the  $\beta$ -form crystalline content, just like the method of orientation drawing of PVDF films [31,32,33] or the introduction of metal particles [34] or nanotubes [35] into the polymer matrix. However, to better exploit this technology, more detailed information about the effect of radiation on the composition of crystalline forms of PVDF is needed. It is not expected that these high energy IR laser irradiation conditions will be present during the typical use of PVDF, but such conditions could be present during the processing of PVDF with such irradiation to generate desirable polymer characteristics. The duration and intensity of the laser used for processing PVDF will vary based on the physical sample characteristics and the desired properties.

In recent years, there has been an increase in interest in the ablation of polymers by use of an infrared (IR) laser due to potential technological uses of this method [36,37]. However, the available results are not sufficient for an accurate description of the physicochemical and thermochemical processes occurring when polymers are exposed to IR laser radiation, so that one can determine the mechanism of polymer degradation. The focus of the current work is on the laser ablation of PVDF under irradiation from a continuous CO<sub>2</sub> laser in a vacuum in order to establish the ablation mechanism.

## **2. Results and Discussion**

### *2.1. Laser ablation – visual observations*

At the beginning of exposing the polymer to the laser beam, the surface layer heats and melts. A characteristic surface microrelief on the areas under the laser beam is formed as the polymer is etched away (Figure 1). A ring of molten PVDF grows around the crater formed during PVDF ablation (Figure 1b). Inside the ring, hot gas flows break through the entire

ablation area. The latter are released in the form of gas bubbles inside the frozen PVDF melt after the laser is turned off (Figures 1b and 1c). The frozen PVDF melt is a foam indicating that the gas flows out not only from the surface of the irradiated zone, but also from the inner points of the surface layer, distributed randomly, forming separate bubbles. With an increase in the duration of laser exposure, the height of the ring growing around the crater increases and the crater deepens. It is characteristic that the melt around the ablation crater has a slightly yellow color at short times of laser exposure, which turns black at long times of laser exposure (Figures 1b and 1c). This indicates carbonization of the polymer macromolecule chain under the IR laser beam.

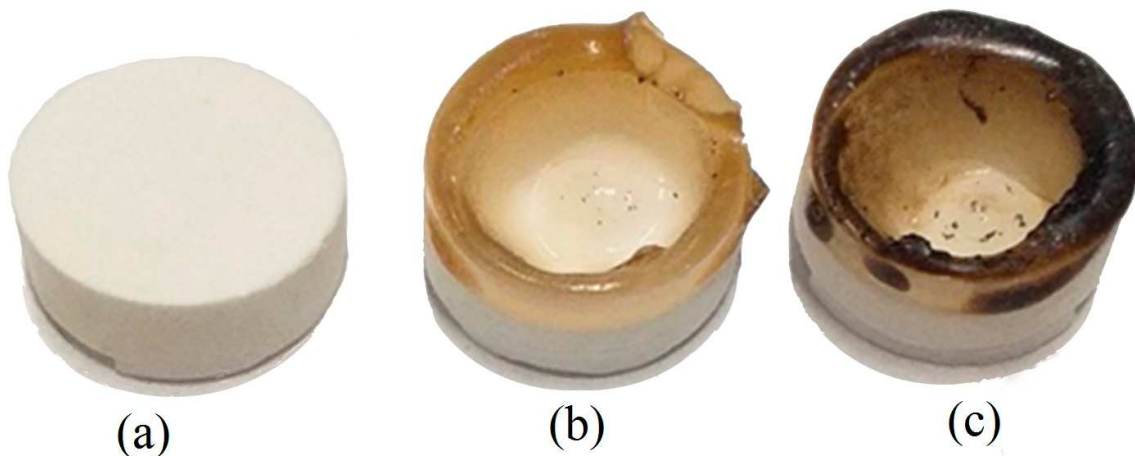


Figure 1. Photographs of the surface of PVDF formed after irradiation with the IR laser. Laser irradiation time (sec): 0 (a), 20 (b), 40 (c).

The dependence of the mass of the evolved gas on the time of laser irradiation is shown in Figure 2. In the initial period of laser exposure (up to 2 sec), the mass of PVDF does not exhibit a significant decrease as the sample is heated to the melting point. As the melted areas are etched away, they form an ablation flow. As a result, the curve of the dependence of the rate of

gas evolution on the time of laser irradiation has a short induction period, and then, the rate of polymer weight loss increases linearly with time of laser irradiation. Thus, the primary heating of the surface and the initiation of decomposition of macromolecules in the molten PVDF layer occurs very quickly. This provides an instant ablative flow of polymer degradation products. When PVDF is exposed to IR laser radiation, the beam energy is converted into the excitation of thermal vibrations. When a sufficient density of the beam power is absorbed by the polymer, dehydrofluorination and fragmentation of macromolecules into chain fragments occurs. Experiments have shown that in the place where the laser beam falls, the polymer glows, i.e. the temperature of the ablation crater is obviously higher than 1000 K, which is much higher than the temperature required for effective thermal destruction of PVDF ( $\geq 703$  K). [38,39,40]

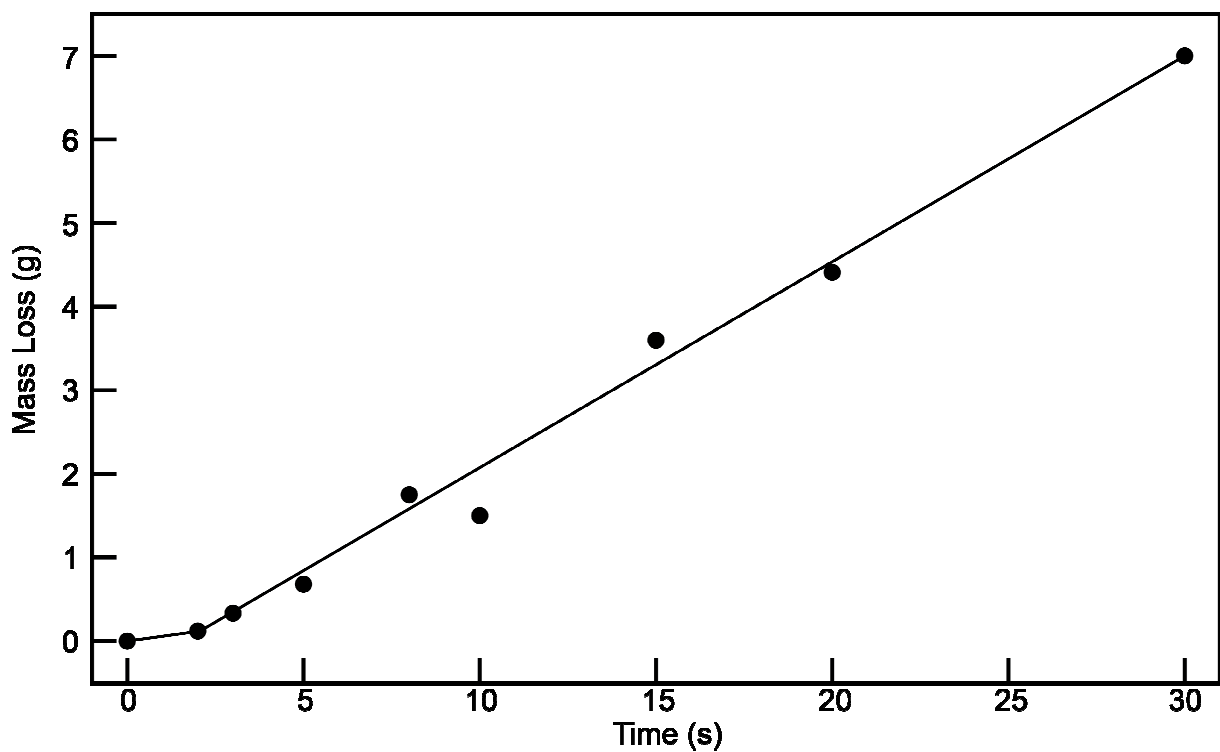


Figure 2. Dependence of the polymer mass loss on the time of exposure to the PVDF laser.

Fragments of macromolecules formed as a result of laser-induced destruction can evaporate together with gaseous ablation products leading to formation of an ablation torch. Most likely, the PVDF ablation torch consists of (1) gaseous, non-condensable components (for example HF, C<sub>2</sub>H<sub>4</sub> and others); (2) components that are gaseous at the temperature of the irradiated target surface, but condense at a lower temperature (for example, oligomeric fragments of macromolecules); and (3) molecular clusters of various sizes (including droplets and strands of melted polymer), which are polymer particles torn out of the target by an intense flow from the first two fractions. Ablation products are carried away with the gas flow. They form a coating deposited on a surface placed in front of the ablation torch. A layer of slightly yellowish powder forms baked onto an aluminum foil substrate.

### *2.1. Laser ablation – mass spectrometry*

The composition of the gaseous products of laser ablation of PVDF, determined by mass spectrometry, is shown in Table 1. The amount of gaseous ablation products beginning with the most prevalent are: HF > C<sub>2</sub>H<sub>4</sub> > CF > CFH<sub>2</sub> > C<sub>2</sub>FH<sub>2</sub> > C<sub>2</sub>FH > > CH<sub>4</sub> ≥ C<sub>2</sub>FH<sub>3</sub> > OH > C<sub>2</sub>H<sub>3</sub> ≥ C<sub>2</sub>H<sub>5</sub> ≥ C<sub>3</sub>F<sub>5</sub>H > CH<sub>2</sub> ≥ C<sub>2</sub>F<sub>2</sub>H<sub>2</sub> > CH<sub>3</sub> ≥ C<sub>3</sub>F<sub>2</sub>H<sub>3</sub> ≥ C<sub>2</sub>F > C<sub>2</sub>F<sub>3</sub> ≥ C<sub>2</sub>H<sub>2</sub> ≥ CF<sub>2</sub>H ≥ C<sub>2</sub>H<sub>6</sub>. HF is the main product of PVDF ablation, formed by dehydrofluorination of the PVDF. The presence of a significant amount of gaseous products among the laser ablation products under the general formula C<sub>x</sub>F<sub>y</sub>H<sub>z</sub> indicates the occurrence of the process of laser-induced destruction of the main PVDF chain.

Table 1. The primary gas products released during the irradiation of PVDF with CO<sub>2</sub> laser radiation.

Mass (a.u.)	Elemental composition	*I/I <sub>C<sub>2</sub>H<sub>4</sub></sub>	Mass (a.u.)	Elemental composition	*I/I <sub>C<sub>2</sub>H<sub>4</sub></sub>
12	C	3.2	45	C <sub>2</sub> FH <sub>2</sub>	32.6
14	CH <sub>2</sub>	7.6	46	C <sub>2</sub> FH <sub>3</sub>	13.0
15	CH <sub>3</sub>	6.5	51	CF <sub>2</sub> H	4.3
16	CH <sub>4</sub>	13.0	53		3.2
19	F	3.2	54		4.3
20	HF	139.1	58	C <sub>3</sub> FH <sub>4</sub>	1.1
26	C <sub>2</sub> H <sub>2</sub>	4.3	60		3.2
27	C <sub>2</sub> H <sub>3</sub>	10.9	63	C <sub>2</sub> F <sub>2</sub> H	2.2
28	C <sub>2</sub> H <sub>4</sub>	100	64	C <sub>2</sub> F <sub>2</sub> H <sub>2</sub>	7.6
29	C <sub>2</sub> H <sub>5</sub>	10.9	65	C <sub>2</sub> F <sub>2</sub> H <sub>3</sub>	3.2
30	C <sub>2</sub> H <sub>6</sub>	4.3	77	C <sub>3</sub> F <sub>2</sub> H <sub>3</sub>	6.5
31	CF	52	78	C <sub>3</sub> F <sub>2</sub> H <sub>4</sub>	2.2
33	CFH <sub>2</sub>	33.7	79	C <sub>3</sub> F <sub>2</sub> H <sub>5</sub>	2.2
39		10.9	81	C <sub>2</sub> F <sub>3</sub>	4.3
40		4.3	132	C <sub>3</sub> F <sub>5</sub> H	10.9
43	C <sub>2</sub> F	6.5	145	C <sub>4</sub> F <sub>5</sub> H <sub>2</sub>	2.2
44	C <sub>2</sub> FH	28.3			

\* - Ratio of the signal intensity of the product (I) to the intensity of the signal from C<sub>2</sub>H<sub>4</sub> (I<sub>C<sub>2</sub>H<sub>4</sub></sub>).

## 2.2. Laser ablation – IR spectroscopy

To better explore the changes in the structure of the PVDF plate that occur under the influence of an IR laser, we compared the IR spectra of the initial polymer and the surface of the polymer irradiated by the laser. The IR spectra of the initial PVDF in Figure 3 and in the Supporting Information show a number of peaks with the positions of the maxima given in Table 2. The interpretation of the position of the maxima of the absorption bands is based on a comparison of the literature IR spectra of PVDF, for example from the IR spectra of a Kynar PVDF sample. [40]

The IR spectra of the products of laser ablation of PVDF are shown in Figure 3 and the Supporting Information. Comparison of the results in Figure 3 for the initial PVDF (spectrum a)

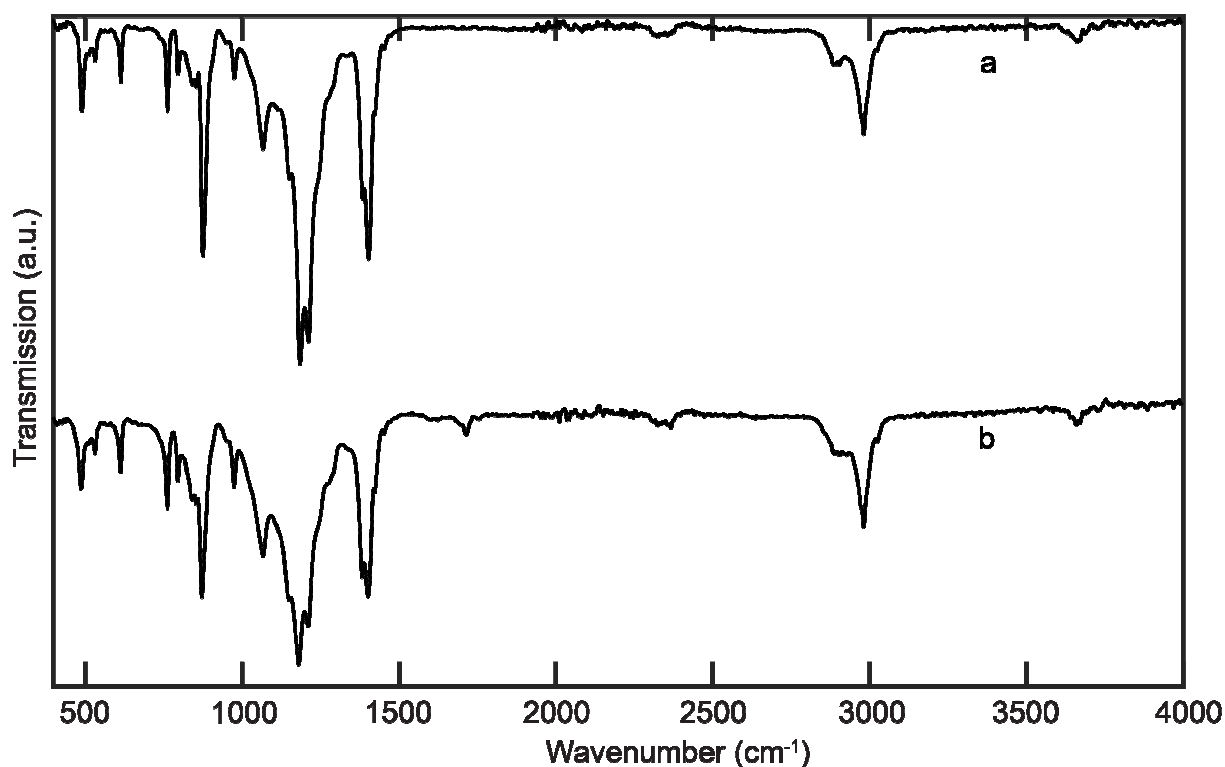


Figure 3. IR spectra of (a) virgin PVDF and (b) PVDF irradiated with IR laser beam for 40 s.

and for the ablation crater ring shown in Figure 1c (spectrum b) shows the presence of new absorption bands in the ablation crater in the region of 1600 to 2366  $\text{cm}^{-1}$  (Table 2). The assignments in Table 2 are based on literature values. [41,42,43,44,45,46] They indicate the presence in the ablation crater of products containing double bonds, cumulated double bonds, and triple bonds. Moreover, this difference in spectra increases with the length of exposure of the polymer surface to the laser (see Supporting Information for longer time spectra). The smallest number of absorption bands are observed in the IR spectrum of the PVDF ablation product extracted from the ablation crater ring formed after irradiation of the polymer with an IR laser for 60 s (Supporting Information). The analysis shows that this sample is essentially a completely

dehydrofluorinated polymer product. The characteristic absorption bands for C-H and C-F bonds practically disappear in this spectrum (Supporting Information). It contains absorption bands characteristic of unsaturated bonds (Table 2).

Table 2. The absorption bands of the virgin and irradiated with IR laser PVDF plates.

Plate	laser ablation Crater	Part of crater	
Frequencies, <sup>a</sup> cm <sup>-1</sup>			Assignment <sup>b</sup>
		377m	(-CH=CF <sub>2</sub> ) (Unsat. Conj. Groups)
	409vw	405m	τ(-CH=CF <sub>2</sub> ) (Unsat. Conj. Groups)
490vw	487vw		r(CH <sub>2</sub> )
532m	532m		r(CH <sub>2</sub> )
612m	612m		r(CH <sub>2</sub> )
740lb	740lb		v <sub>s</sub> (CF <sub>2</sub> )
763m	763m		δ(CF <sub>2</sub> )+δ(CCC)
796m	796m		τ(CH <sub>2</sub> )
842vw	841vw	841m	τ(CH <sub>2</sub> )-v <sub>a</sub> (CF <sub>2</sub> )
855w	854vw		v <sub>a</sub> (CC)+v <sub>s</sub> (CF <sub>2</sub> )
875s	875s		
952lb	952lb		
975m	975m		τ(CH <sub>2</sub> )
		995vw	δ(CH)(Unsat. Conj. Groups), v(C-C≡C)
1068s	1068s		v <sub>a</sub> (CC)-ω(CF <sub>2</sub> )+ ω(CH <sub>2</sub> )
		1117vw	τ(CH <sub>2</sub> )
1148lb	1148lb		v <sub>s</sub> (CF <sub>2</sub> )
1185s	1181s		v <sub>s</sub> (CF <sub>2</sub> )+τ(CH <sub>2</sub> )
1212m	1211m		v <sub>a</sub> (CF <sub>2</sub> )+ω(CH <sub>2</sub> )
1243lb	1243lb		v <sub>a</sub> (CF <sub>2</sub> )+ω(CH <sub>2</sub> )
1287ld	1287lb		v <sub>s</sub> (CF <sub>2</sub> )-v <sub>s</sub> (CC)+ δ(CCC)
1384lb	1383lb		δ(CH <sub>2</sub> )+ω(CH <sub>2</sub> )
1403s	1402s		ω(CH <sub>2</sub> )-v <sub>a</sub> (CC)
1423lb	1423lb		δ(CH <sub>2</sub> )-ω(CH <sub>2</sub> )
1454vw	1453vw		δ <sub>a</sub> (CH <sub>3</sub> )
	1599vw	1587m	(C=C- C=C)
	1623vw		v(C=C)
	1686 lb		v(C=C)
	1714w		v(-CH=CF <sub>2</sub> )
	1700 lb	1707vw	ω(=CH <sub>2</sub> ) in >C=C=CH <sub>2</sub>
	1755vw		v(>C=CF <sub>2</sub> )

	2011vw	2000vw	$\nu_a(\text{C}=\text{C}=\text{C})$
	2036vw	2083vw	$(\text{C}\equiv\text{C})$ Conjugated with $\text{C}=\text{C}$ or $\text{C}\equiv\text{C}$
		2157w	$\nu(-\text{C}\equiv\text{CH})$
	2366w		$\nu(\text{CH})$ (in $-\text{C}\equiv\text{CH}$ )
2902vw	2902vw		$\nu(\text{CH}_2)$ , $\nu(\text{CH}_3)$
2926vw	2926vw		$\nu_a(\text{CH}_2)$
2972lb	2972lb		$\nu_a(\text{CH}_3)$
2981s	2981s		$\nu_s(\text{CH}_2)$
3023m	3024m		$\nu_a(\text{CH}_2)$
3661w	3658w		$\nu(\text{OH})$

<sup>a</sup>Relative intensity: s = strong, m = medium, w = weak, vw = very weak, lb = line bend.

<sup>b</sup>Type of vibration:  $\nu_a$  – antisymmetric stretching vibrations,  $\nu_s$  – symmetric stretching vibrations,  $\omega$  – “wagging” vibrations,  $\delta$  – deformation vibrations,  $\tau$  – torsion vibrations. The signs “+” and “-“ show the phase relationship.

#### 2.4. Supramolecular structure of the laser ablation products condensed at 300 K.

In addition to low molecular weight molecules and their fragments, the PVDF ablation flow contains high molecular weight microaggregates representing microdroplets of a polymer melt. They are formed by entrapment of a polymer melt in a hot turbulent flow of gaseous decomposition products escaping from the subsurface layer through microcraters. After collision with the substrate surface and solidification, these particles form spherical aggregates, as well as an underlying film.

Figure 4 shows SEM pictures of a powder coating (a) formed from the flow of products of an ablation torch. Spherical particles with an average diameter of about 100 nm are formed. The shape and size of particles formed from a polymer melt usually depends on the specific surface tension of the melt (free surface energy). The higher the free surface energy, the more rounded and smaller the particles become.

It is known [47] that in a nonequilibrium regime, fragments of macromolecules with radical character can be carried away. In general, they have a chemical structure close to that of the original polymer. Condensing on a cold substrate (about 300 K), such large fragments of the PVDF macro-chain combine with each other to form an ablation product close in composition to

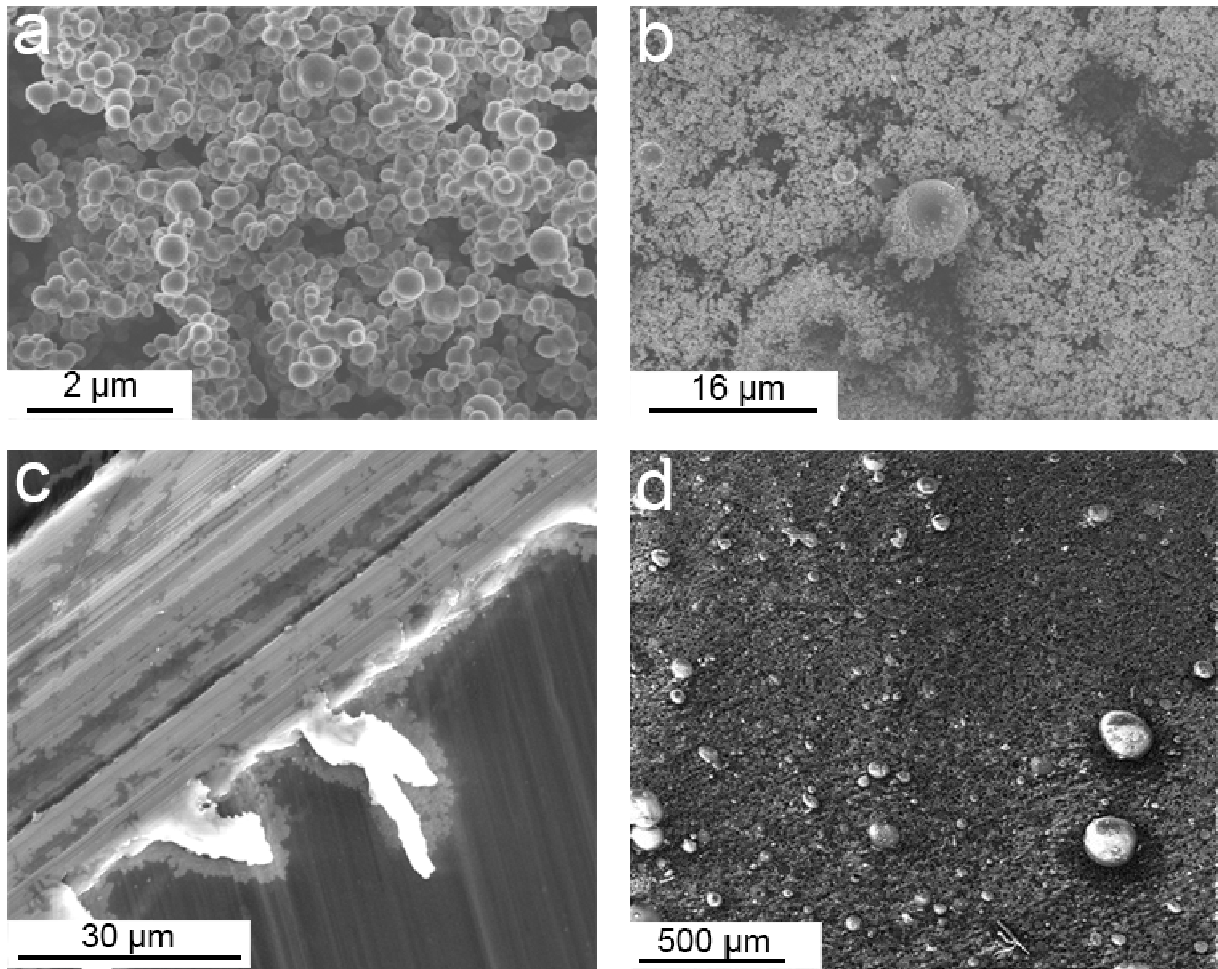


Figure 4. Pictures of an SEM of coating formed from a plume of PVDF laser ablation products.

In picture d is shown needle scratch marks.

the initial polymer. The mobility of fragments of macromolecules on the substrate leads to the formation of dendritic type structures, similar to those of treelike corals (Figure 4b). The similarity of the spherical particles in Figure 4a suggests their formation from smaller particles,

which are oligomeric fragments of macromolecules. The coating material when scratched (Figure 4c) behaves like paraffin, most likely due to its low molecular weight. Simultaneously with the formation of the coating by polymerization of the condensed fraction, a flow of droplets is deposited on the substrate, consisting of shaped aggregates with a diameter from several units to several hundred micrometers (Figure 4d). The droplets have a regular spherical shape and a smooth surface, consistent with an origin from a superheated polymer melt. Large structures are visible among the droplets, but they are often found under the finer droplet fraction. In the course of laser ablation on the already formed surface of droplets from a large (diameter 10-30  $\mu\text{m}$ ) and medium fraction (diameter 1-5  $\mu\text{m}$ ), smaller droplets of polymer melt settle as shown in Figures 5b and 5d. Thus, the coating shown in Figure 4 is formed as a result of two parallel processes: (1) the formation of a dendritic coating by the condensation of products from the gas phase; and (2) the splashing and entrainment of melt droplets.

The shape and size of the particles formed from the polymer melt under the laser ablation will depend on the specific surface tension of the polymer melt (free surface energy). The high free surface energy of melts leads to the formation of particles that have more of a spherical shape and are of smaller sizes. The free surface energy of PVDF is 39.6 mN/m [48] which is consistent with the formation of spherical particles of regular shape with a low average diameter of about 100 nm from the melt in PVDF. The particle size distribution histogram is shown in Figure 5.

The dimensional composition of the resulting coating is polydisperse and contains both small size fractions from 50 nm, and agglomerates of tightly bound particles, the size of which can be up to 300 nm. This powdery underlying film is formed due to the condensable fraction of

laser ablation products, consisting of relatively long fragments of the chain of PVDF macromolecules, which are volatile at temperatures  $\geq 1000$  K.

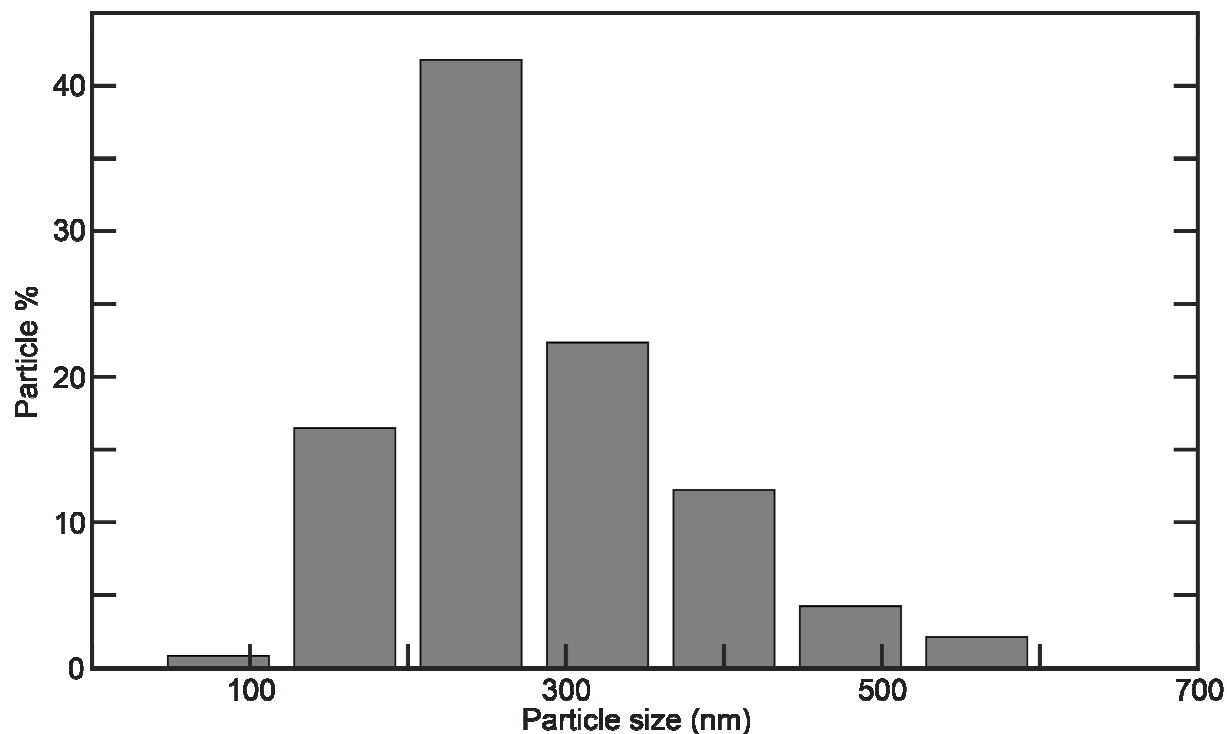


Figure 5. Histogram of the particle distribution of the coating obtained by laser ablation of PVDF.

### 2.5. Mechanism of PVDF laser ablation.

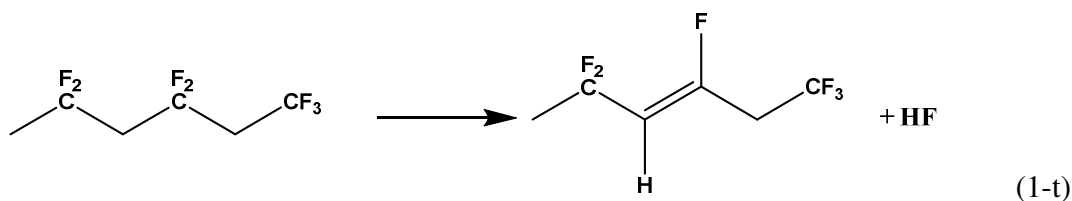
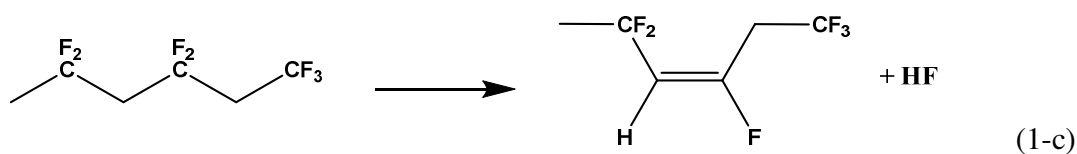
Mass spectrometric analysis of the gaseous products of PVDF ablation showed the releasing a large amount of hydrogen fluoride as a result of dehydrofluorination (Table 1). In order to develop a mechanism, reaction thermodynamics and selected transition state energies were calculated at the G3(MP2)B3 level (Table 3). The presence of alternating  $\text{CH}_2$  and  $\text{CF}_2$  groups in PVDF makes it possible that complete dehydrofluorination could occur while preserving the carbon skeleton which would lead to the formation of carbinoid structures. Our

model for the PVDF polymer is  $\text{CH}_3\text{CF}_2\text{CH}_2\text{CF}_2\text{CH}_2\text{CF}_3$  and this is used in the calculated reactions.

Table 3. Reaction enthalpies ( $\Delta\text{H}$ ) and free energies ( $\Delta\text{G}$ ) for HF loss and associated reactions in kcal/mol calculated at G3(MP2)B3 with reaction enthalpy and free energy barriers presented as  $\Delta\text{H}^\ddagger$  and  $\Delta\text{G}^\ddagger$  respectively.

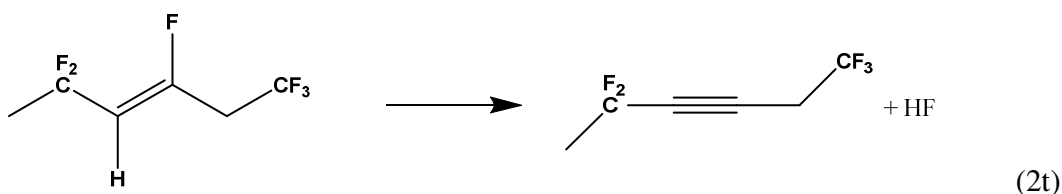
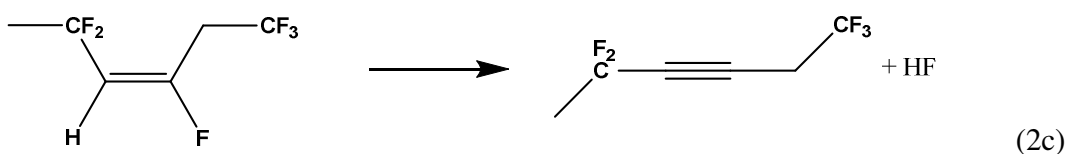
Rxn #	$\Delta\text{H}$	$\Delta\text{G}$	$\Delta\text{H}^\ddagger$	$\Delta\text{G}^\ddagger$
1-c	15.9	5.1	60.3	60.5
1-t	15.7	4.6	62.9	62.8
2-c	24.7	13.0	74.3	73.2
2-t	24.8	13.4	73.5	72.0
3a-c	33.8	22.5	70.1	70.2
3a-t	34.0	22.9	70.1	69.2
3b-c	23.6	12.6	71.3	71.0
3b-t	23.7	13.0	71.3	71.3
4	91.7	76.9		
5a	-64.5	-62.6	12.6	25.0
5b	-72.9	-70.2	39.2	49.4
6	56.8	44.3		
7	100.8	89.3		
8	-172.3	-160.1		
9	-129.5	-117.7		
10	-67.8	-55.0		
11	-4.3	-7.2		
12	37.9	35.7		
13	-8.1	-9.7		
14	30.5	28.8		
15	-2.5	-2.5		
16	43.1	33.5	86.3	85.7

The process of dehydrofluorination of PVDF under an IR laser beam could include reactions in two time domains. In the initial time domain, unimolecular decomposition by removal of HF leads to polyene structures (reaction 1) with c = cis and t = trans.

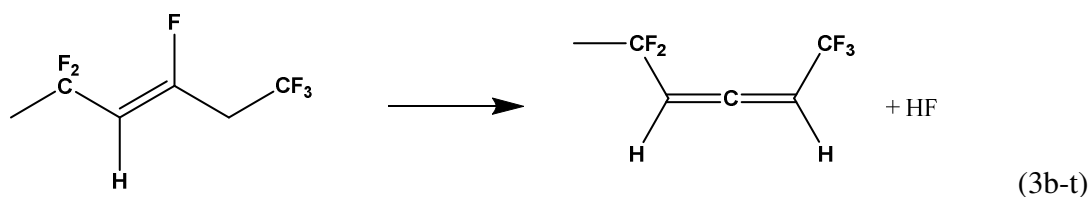
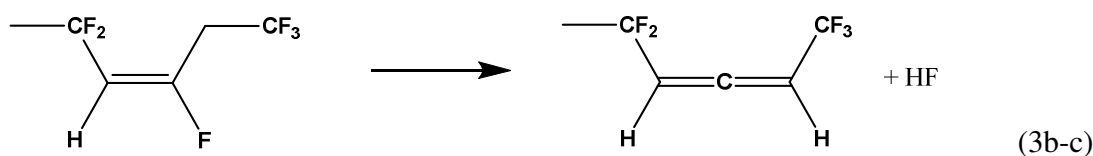
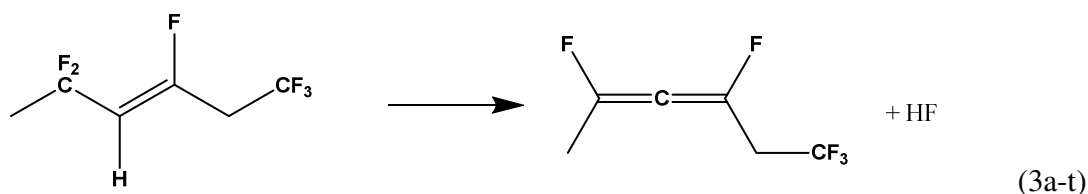
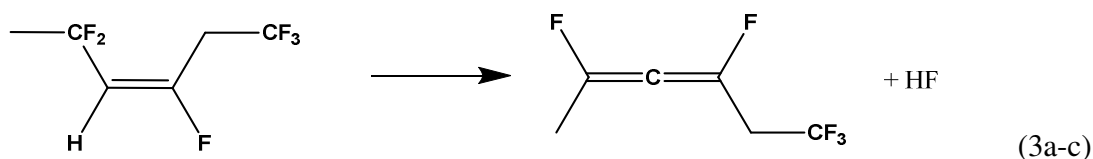


The thermodynamics for production of cis and trans isomers, reactions (1c) and (1t), are essentially identical with differences within chemical accuracy ( $\pm 1$  kcal/mol). Production of the cis isomer has a slightly lower transition state energy barrier. Although the free energy is only slightly endergonic,  $\sim 5$  kcal/mol at 298 K, the transition state energy barrier of  $\sim 60$  kcal/mol will hinder this reaction from occurring at either low laser power or moderate temperature. Increasing the temperature will lead to more HF production both kinetically and thermodynamically.

Subsequent unimolecular dehydrofluorination leads to formation of alternating triple C $\equiv$ C and single C-C bonds (reactions (2c) and (2t) depending upon the stereoisomer of the initial loss of HF), or the formation of cumulenes (reactions (3a-c to 3b-t) depending on the starting cis or



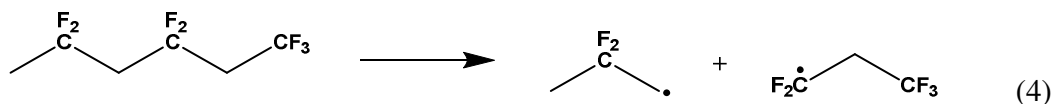
trans structure and whether F substituents or H substituents are present on the C atoms at the end of the cumulene.)



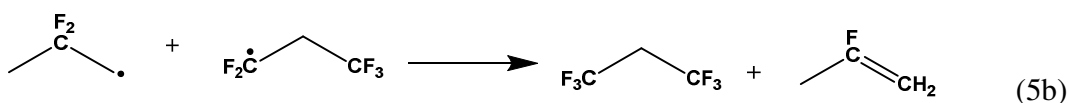
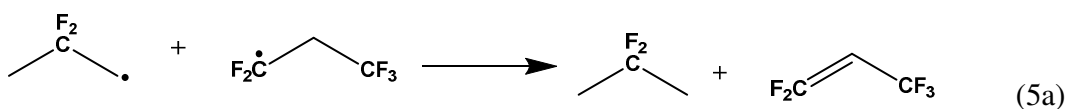
Thermodynamically reactions (2) and reactions (3b) are more endothermic than reactions (1) by ~10 kcal/mol and are less endothermic than reactions (3a) by ~10 kcal/mol. However, the transition state energy barriers for reactions (2) and (3) are within 3 kcal/mol of one another so the kinetics will be comparable. The energy barriers for reactions (2) and (3) are more than 10 kcal/mol higher than for reactions (1). No meaningful energy differences were found between cis- and trans- starting products for reactions (2), (3a), and (3b), just as for reactions (1). The unsaturated bonds formed as a result of dehydrofluorination in the polymer chain contribute to the coloring of the laser-irradiated part of the polymer. The initial white color of the polymer gradually changes, first to yellow, and then to brown and black, with an increase in the time of laser action on the polymer as a result of the accumulation of various chromophore groups in the polymer structure (C=C, C≡C). The change in color of PVDF from white to black with an

increase in the time of exposure to the laser on the polymer is consistent with carbonization of the polymer chain due to IR irradiation.

The largest change in the polymer color as a result of ablation is observed on the rings on the rings on the edges of the ablation crater. In the well of the ablation crater, where the part of the polymer degraded under the laser beam escapes together with the gas ablation products, the degree of coloration is noticeably lesser than on the crater rings. The formation and increase in the number of multiple bonds leads to an increase in conjugation. As a result, the polymer surface is carbonized and becomes more heat resistant. These features contribute to an increase in the absorption of laser radiation and to an increase in the temperature of the absorption layer. As a result, the temperature of the polymer target can reach the temperature of thermal decomposition of C-C bonds, and macroradicals are formed, first in a cage as given by reaction (4).

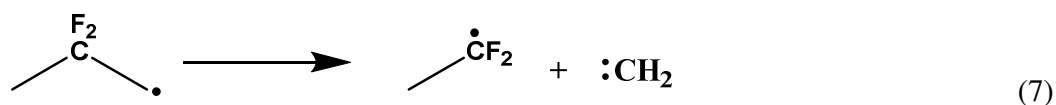
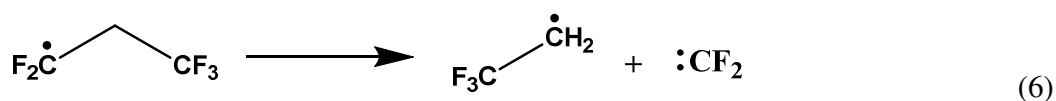


Thermodynamically, reaction (4) should only occur where bond unsaturation already exists, as the C-C bond dissociation energy (BDE) ( $\Delta G_{298} = 77$  kcal/mol) represented by reaction (4) is greater than the activation energies for reactions (1) to (3). Subsequent disproportionation of radicals in the cage as a result of the attack of the  $\sim\text{CF}_2\text{-CH}_2\text{-C}\cdot\text{F}_2$  radical on the C-H-bond of the  $\text{C}\cdot\text{H}_2\text{-CF}_2\text{-CH}_2\sim$  radical (or vice versa) leads to the formation of terminal unsaturated bonds.



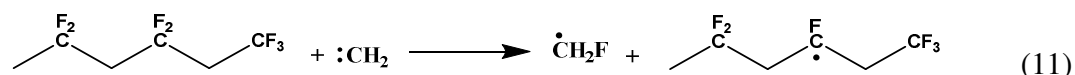
Both reactions (5a) and (5b) are extremely exergonic with reaction (5a) having a low energy barrier but reaction (5b) has an energy barrier ~25 kcal/mol higher than that of reaction (5a) due to the greater energy required to transfer a F atom instead of an H atom between the two molecules and the fact that the single electron on the F atom lone electron is in a p orbital. Such a loss of C-C bonds will lead to the destruction of the polymer chain and the formation of chains of shorter length than in the initial PVDF macromolecule.

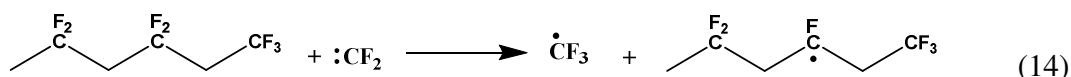
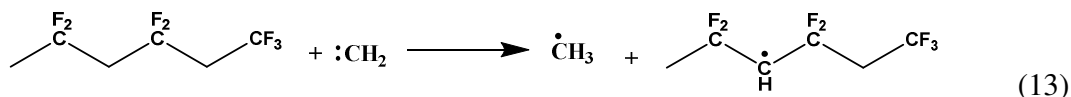
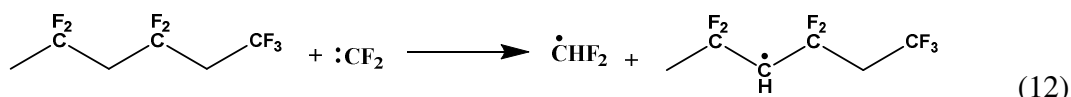
Since the laser ablation process can lead to rather high temperatures, the radicals formed in Reaction (4) can undergo thermal decomposition by loss of carbenes with :CF<sub>2</sub>, a singlet, and :CH<sub>2</sub>, a triplet :



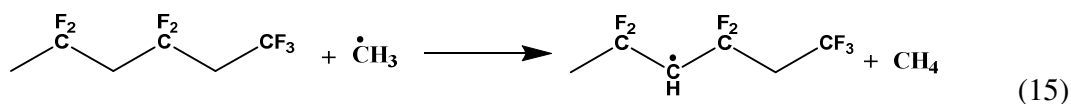
Reaction 6 is far less endothermic than reaction 7 (~45 kcal/mol) due to the stability of the singlet carbene :CF<sub>2</sub>.

The analysis of the laser polymer products listed in Table 1 indicates that the predominant part of the ablation gas products apparently arise from secondary reactions with the participation of generated carbenes such as shown in Reactions (8) to (14).





Reactions (8) to (10) are both exoergic. Reactions (8) and (9) are extremely exoergic due to high energy triplet  $\text{:CH}_2$  reacting to form a singlet product. Reactions (11) and (13) are also exoergic due to the reactions having triplet  $\text{:CH}_2$  as a reactant whereas reactions (12) and (14) are endoergic due in part to the more stable singlet  $\text{:CF}_2$  reactant. The products obtained in these reactions can participate in other reactions during the ablation process. For example, the methyl radical formed in Reaction (13) can remove a hydrogen atom from the PVDF macromolecule and form methane in the exoergic reaction (15).



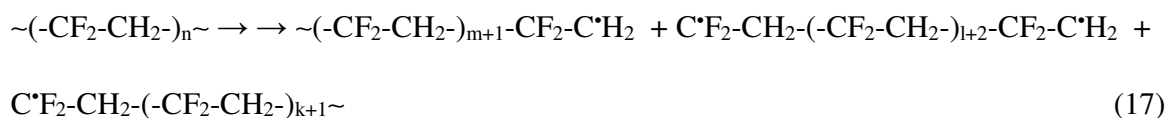
The vinylidene fluoride molecule formed in reaction (9) can be thermally dehydrofluorinated transforming into the reactive monofluoroacetylene, an endoergic reaction with the highest transition state energy barrier of the reactions studied:



which is also one of the main gaseous products of PVDF ablation.

The composition of the coating formed during laser ablation of PVDF contains droplets of polymer melt deposited on the cooled surface outside the zone of laser action. Melt droplets contain relatively small pieces of macromolecules that are gases at the ablation temperature, but

transform into a condensed state at 300 K. They are formed as a result of breaking two or more C-C bonds of one polymer chain as represented by reaction (17).



where  $n=m+k+1$ .

After condensation on a cold substrate, the resulting radicals will easily recombine with other similar fragments or other radical ablation products. If a fragment is long enough to act as a flexible chain, it could cyclize leading to chain termination, but entropy effects will be unfavorable at high temperatures. Rearrangement of the resulting radicals by migration of a hydrogen atom along the chain is unlikely as it is hindered by the fluorine atoms in the chain. Due to the high temperature in the reactor, decay or disproportionation of radicals is possible. As a result, terminal unsaturated bonds are formed in the composition of the products forming the coatings. The IR spectra of the coating indicate the presence of such end fragments in the composition of the coating products.

### 3. Conclusions

IR laser irradiation of PVDF results in crater formation paired with discoloration that increases as the ablation time increases. Under the laser ablation conditions that were used, the initial period of exposure (2 seconds) melts the polymer without significant mass change. Following this induction period, the mass loss with respect to ablation time increased linearly. The primary gaseous products produced during ablation are HF and  $\text{C}_x\text{F}_y\text{H}_z$  (where  $x \geq 2$ ) indicating that both polymer backbone unsaturation and cleavage occur. FTIR spectroscopy of ablated PVDF showed the formation of unsaturation (double bonds, cumulated double bonds, and triple bonds) on the surface. As the laser ablation time increases to 60 seconds, the

characteristic C-H and C-F absorption bands disappear indicating a significantly dehydrofluorinated product. As a result of laser ablation, a fine powder was found to coat the PVDF surface. This powder was a result of either ablation induced hot gas flow depositing polymer microdroplets outside the ablation crater or formation of surface protrusions via deposition of radical containing polymer fragments reacting in the gas phase. The resulting particles are generally spherical with 50-300 nm diameter.

Reaction thermodynamics and selected transition state barrier energies were calculated at the G3(MP2)B3 level. Initial dehydrofluorination requires high temperature or laser power to be both thermodynamically and kinetically feasible. Kinetically, subsequent HF loss will lead to either triple bonded or cumulated carbons. Backbone bond breaking should only occur once unsaturation is present and leads to radical disproportionation causing backbone degradation and further unsaturation. The experimentally observed gaseous ablation products are likely caused by secondary reactions with carbenes (:CH<sub>2</sub> and :CF<sub>2</sub>) and the subsequent products of these reactions can react further.

The IR laser irradiation processing conditions used in this work were done for a range of times. This range of ablation times was necessary as the degradation curve with respect to time is a key characteristic for future work to improve the characteristics of PVDF via laser ablation as a processing tool. The minimization of PVDF dehydrofluorination during laser ablation to achieve the desired material properties is a topic that warrants further study. One possible method for limiting dehydrofluorination is to raster the beam over the sample to manage local heating of the polymer surface.

## **4. Experimental and Computational Methods**

### *4.1. Materials*

The PVDF powder with a molecular weight  $M_n = 534000$  g/mol was purchased from Aldrich (CAS 24937-79-9). The samples of the polymer target under laser irradiation were cylindrical pellets that are 10 mm in diameter and 6 mm in height. They were made by pressing powdered PVDF in a mold at an optimized pressure of 20 MPa at room temperature.

#### *4.2. Laser Irradiation of PVDF*

The process of laser ablation (LA) was carried out in a vacuum chamber system previously described in detail. [38] A continuous CO<sub>2</sub> laser “LGN-703” with a wavelength of 10.6  $\mu\text{m}$ , power of 40 W, and diameter of the laser beam at the target surface of 9 mm was used. A window made from a single crystal of sodium chloride was used to pass the laser beam into the ablation chamber. Before the experiment, the laser was turned on for 5 min to stabilize the laser power and the mode structure of the beam. The laser ablation chamber was evacuated initially up to  $(1.5-4) \times 10^{-4}$  Pa. The ablation process was also performed with continuous evacuation of the gaseous products of laser ablation. The condensed ablation products and microparticles of the degraded polymer entrained by the intense gas flow were deposited on the surface of an aluminum foil mounted 50 mm from the target surface.

#### *4.3. Mass spectrometric analysis*

The analysis of the gaseous products of the polymer laser ablation was carried out using an MX-7304 quadrupole mass spectrometer. Non-condensable decomposition products were fed through a 12 mm diameter, 500 mm long pipe to a quadrupole mass spectrometer with its own vacuum system consisting of a mercury diffusion pump with a nitrogen trap and a magnetic ionization sensor. Before a measurement, the mass spectrometer was evacuated to a pressure of  $(1.5 \text{ to } 4) \times 10^{-5}$  Pa. During the mass spectral analysis, the vacuum chamber was disconnected from pumping and connected to the mass spectrometer. At the same time, the pressure in the

mass spectrometer increased to  $(5 \text{ to } 8) \cdot 10^{-5}$  Pa and remained constant during the period of recording the mass spectrum. The presence of a high-vacuum mercury pump in the mass spectrometer made it possible to easily control the quality of the mass spectrum due to the presence of 6 high-intensity isotopes with a mass of 198-204 amu in mercury.

#### *4.4. FT-IR spectrometric analysis*

Infrared spectra of PVDF before and after laser irradiation were recorded for 16 scans in the frequency range 400 to 4000  $\text{cm}^{-1}$  on a Bruker ALPHA Fourier spectrometer equipped with a detached total internal reflection attachment with a single reflection diamond prism (ATR, FTIR-ATR) at  $T = 23$  °C.

#### *4.5. Scanning electron microscopy*

The supramolecular structure of the samples with deposited ablation products was measured using a SUPRA25 field emission scanning microscope (Carl Zeiss, Germany).

#### *4.6 Computational Methods*

Molecular geometries were first optimized at the density functional theory (DFT) level with the B3LYP functional [49,50] and the DZVP2 basis set. [51] Frequency calculations were performed to ensure that the geometry was a transition state or energy minimum. The B3LYP/DZVP2 optimized geometries were used as the initial geometries for the composite, correlated G3(MP2)B3 molecular orbital theory level calculations. [52] All calculations were performed using Gaussian16. [53]

#### **Declaration of Competing Interest**

The authors declare no competing financial interest. The experimental work was performed at the Institute of Problems of Chemical Physics of the Russian Academy of Sciences,

Chernogolovka. The computational work was performed at The University of Alabama. All authors contributed to the data analysis and to writing the manuscript.

### **Acknowledgements**

The reported study was funded by the Russian Foundation for Basic Research under Project No. 19-33-90004. The experimental work was carried out within the framework of state contracts no. AAAA-A19-119041090087-4 and AAAA-A19-119071890015-6. The computational work was supported by the U.S. Department of Energy (DOE), Office of Science, Office of Basic Energy Sciences, Chemical Sciences, Geosciences, and Biosciences Division, Catalysis Center program, at The University of Alabama (DAD) via a subcontract from the Pacific Northwest National Laboratory. D.A.D. thanks the Robert Ramsay Fund at The University of Alabama for support.

## References

- 
- <sup>1</sup> J. Scheirs, *Modern Fluoropolymers*, Wiley, Chichester, 1997.
  - <sup>2</sup> J. G. Drobny, *Technology of Fluoropolymers*, 2nd ed. CRC Press: Boca Raton, FL, USA, 2008.
  - <sup>3</sup> B. Ameduri, *Chem Rev.* 109 (2009) 6632-6686.
  - <sup>4</sup> G. Hougham, P. E. Cassidy, K. Johns, J. Davidson *Fluoropolymers: Synthesis and Applications*. Vol. 1 and 2, Plenum: New-York, 1999.
  - <sup>5</sup> A.J. Lovinger. In: D.C. Basset (Ed.), *Developments in Crystalline Polymers*, Applied Science Publications, London, 1981.
  - <sup>6</sup> M. Tazaki, R. Wada, M. Okabe, T. Homma, *J. Appl. Polym. Sci.*, 65 (1998) 1517-1524.
  - <sup>7</sup> W. K. Lee, C. S. Ha, *Polymer*, 39 (1998) 7131-7134.
  - <sup>8</sup> A. Salimi, A.A. Yousefi, *Polym. Test*, 22 (2003) 699-704.
  - <sup>9</sup> V. Sencadas, R. Gregorio Jr., S. Lanceros-Méndez, *J. Macromol. Sci. Part B: Phys.*, 48 (2009) 514-525.
  - <sup>10</sup> Uy. A. Panshin, S. G. Malkeevich, Z. S. Dunaevskaya, *Ftoroplasti (Fluoroplasts)*, Khimiya, Leningrad, 1978. (in Russ.).
  - <sup>11</sup> V. S. Ivanov, *Radiation Chemistry of Polymers*, VSP, Leiden, 1992.
  - <sup>12</sup> . L. A. Pesin, V. M. Morilova, D. A. Zhrebtsov, S. E. Evsyukov, *Polym. Degrad. Stab.*, 98 (2013) 666-670.
  - <sup>13</sup> Y. M. Lim, P. H. Kang, S.M. Lee, S.S. Kim, J.P. Jeun, C. H. Jung, J. H. Choi, Y. M. Lee, Y.C. Nho, *J. Ind. Eng. Chem.*, 12 (2006) 589-593.
  - <sup>14</sup> Z. Tan, X. Wang, C. Fu, C. Chen, X. Ran, *Radiat. Phys. Chem.*, 114 (2018) 48-55.
  - <sup>15</sup> Yu. A. Ol'khov, S. R. Allayarov, I. N. Shtefan, Yu. N. Smirnov, D. A. Dixon, *High Energy Chem.*, 46 (2012) 336-342.

- 
- <sup>16</sup> L. Dumas, B. Albela, L. Bonneviot, D. Portinha, E. Fleury, *Rad. Phys. Chem.*, 86 (2013) 110-117.
- <sup>17</sup> I. Yoshinobu, K. Shunichi, H. Shinji, *Bull. Chem. Soc. Jpn.*, 71 (1998) 2721-2725.
- <sup>18</sup> M. D. Duca, C. L. Plosceanu, T. Pop, *J. Appl. Polym. Sci.*, 67 (1998) 2125-2129.
- <sup>19</sup> A. Le Moël, J.P. Duraud, C. Lecomte, M.T. Valin, M. Henriot, C. Le Gressus, C. Darnez, E. Balanzat, C.M. Demanet, *Nucl. Instrum. Methods Phys. Res. B.*, 32 (1988) 115-119.
- <sup>20</sup> E.H. Adem, S.J. Bean, C.M. Demanet, A. Le Moel, J.P. Duraud, *Nucl. Instrum. Methods Phys. Res. B.*, 32 (1988) 182-185.
- <sup>21</sup> Yu. A. Ol'khov, S. R. Allayarov, K. I. Muntele, D. A. Dixon, *High Energy Chem.*, 48 (2014) 144-151.
- <sup>22</sup> E. Adem, J. Rickards, E. Munoz, G. Burillo, L. Cota, M. Avalos-Bora, *Rev. Mexicana Fis.*, 49 (2003) 537-541.
- <sup>23</sup> S. R. Allayarov, Yu. A. Ol'khov, I. N. Shtefan, K. I. Muntele, D. Ila, D. A. Dixon, *High Energy Chem.*, 46 (2012) 84-90.
- <sup>24</sup> Yu. A. Ol'khov, S. R. Allayarov, C. I. Muntele, D. A. Dixon, *High Energy Chem.*, 48 (2014) 133-136.
- <sup>25</sup> 19. S.R. George, J.A. Leraas, S.C. Langford, J.T. Dickinson, *Appl. Surf. Sci.*, 255 (2009) 9558-9561.
- <sup>26</sup> Y. Ji, J. Liu, Y. Jiang, Y. Liu, *Spectro. Acta Part A.*, 70 (2008) 297-300.
- <sup>27</sup> A. Bartnik, H. Fiedorowicz, R. Jarocki, J. Kostecki, M. Szczurek, P.W. Wachulak, *Appl Phys A.*, 106 (2012) 551-555.
- <sup>28</sup> S. R. Allayarov, L. A. Kalinin, E. M. Tolstopyatov, P. N. Grakovich, L. F. Ivanov, D. A. Dixon, *J. Russ. Laser Res.*, 38 (2017) 364-368.

- 
- <sup>29</sup> Y. Rosenberg, A. Siegmann, M. Narkis, S. Shkolnik, *J. Appl. Polym. Sci.*, 45 (1992) 783-795.
- <sup>30</sup> S. R. Allayarov, Y. A. Olkhov, D. A. Dixon, *J. Russ. Laser Res.*, 38 (2017) 482-489.
- <sup>31</sup> G. T. Davis, J. E. McKinney, M. G. Broadhurst, S. C. Roth, *J. Appl. Phys.*, 149 (1978) 4998.
- <sup>32</sup> A. Salimi, A. Yousefi, *J. Polym. Sci.*, 42 (2004) 3487-3495.
- <sup>33</sup> T. Lei, L. Yu, G. Zheng, L. Wang, D. Wu, D. Sun, *J. Mater. Sci.*, 50 (2015) 4342-4347.
- <sup>34</sup> S. Yoon, A. Prabu, K. Kim, C. Park, *Macromol. Rapid. Commun.*, 29 (2008) 1316-1321.
- <sup>35</sup> L. Yu, P. Cebe, *Polymer*, 50 (2009) 2133-2141.
- <sup>36</sup> Yu. A. Ol'khov, S. R. Allayarov, E. M., Tolstopyatov, P. N. Grakovich, L. A. Kalinin, Yu. A. Dobrovol'skii, D. A. Dixon. *High Energy Chem.*, 44 (2010) 63-74.
- <sup>37</sup> P. N., Grakovich L. F. Ivanov, L. A. Kalinin, I. L. Ryabchenko, E. M. Tolstopyatov, A. M. Krasovskii. *Russ. J. Gen. Chem.*, 79 (2009) 626-634.
- <sup>38</sup> M. Wang, J.H. Shi, K.P. Pramoda, S.H. Goh, *Nanotechnology*, 18(2007) 235701.
- <sup>39</sup> E. Giannetti, *Polymer Int.*, 50 (2001) 10-26.
- <sup>40</sup> S. R. Allayarov., L. A. Kalinin, D. A. Dixon, E. M., Tolstopyatov, I. A. Frolov, L. F. Ivanov, P. N. Grakovich, O. N. Golodkov, *J. Russ. Laser Res.*, 40 (2019) 356-363.
- <sup>41</sup> G. Socrates. *Infrared and Raman Characteristic Group Frequencies: Tables and Charts*. Third Edition. John Wiley & Sons, LTD: Chichester. New York. Weinheim. Toronto. Brisbane. Singapore. 2004. 366 C.
- <sup>42</sup> J. Mihály, S. Sterkel, H. M. Ortner, L. Kocsis, L. Hajba, É. Furdyga, J. Mink, *Croat. Chem. Acta.*, 79 (2006) 497-501.
- <sup>43</sup> Y. Peng, P. Wu, *Polymer*, 15 (2004) 5295-5299.
- <sup>44</sup> V. V. Kochervinsky, *Russ. Chem. Rev.*, 65 (1996) 865-913.

- 
- <sup>45</sup> D. L. Pavia, G. M. Lampman, G. S. Kriz, J. R. Vyvyan, *Introduction to Spectroscopy*, 5th ed., Cengage Learning, Independence, KY, USA 2015.
- <sup>46</sup> E. F. Il'icheva, H. A. Slovokhotova, I. G. Akhvlediani, *Polymer Sci. U.S.S.R.*, 18 (1976) 242-250.
- <sup>47</sup> V. S. Pudov, A. L. Buchachenko, *Russ. Chem. Rev.*, 39 (1970) 70-84.
- <sup>48</sup> I. F. Shaimukhametova, S. A. Bogdanova, S. R. Allayarov, D. A. Dixon, *High Energy Chem.*, 55 (2021) (in print).
- <sup>49</sup> A. D. Becke, *J. Chem. Phys.*, 98 (1993) 5648-5652.
- <sup>50</sup> C. Lee, W. Yang, R. G. Parr, *Phys. Rev. B*, 37 (1988) 785-789.
- <sup>51</sup> N. Godbout, D. R. Salahub, J. Andzelm, E. Wimmer, *Can. J. Chem.*, 70 (1992) 560-571.
- <sup>52</sup> A. G. Baboul, L. A. Curtiss, P. C. Redfern, K. Raghavachari, *J. Chem. Phys.*, 110 (1999) 7650-7657.
- <sup>53</sup> M. J. Frisch, G. W. Trucks, H. B. Schlegel, G. E. Scuseria, M. A. Robb, J. R. Cheeseman, G. Scalmani, V. Barone, G. A. Petersson, H. Nakatsuji, X. Li, M. Caricato, A. V. Marenich, J. Bloino, B. G. Janesko, R. Gomperts, B. Mennucci, H. P. Hratchian, J. V. Ortiz, A. F. Izmaylov, J. L. Sonnenberg, D. Williams-Young, F. Ding, F. Lipparini, F. Egidi, J. Goings, B. Peng, A. Petrone, T. Henderson, D. Ranasinghe, V. G. Zakrzewski, J. Gao, N. Rega, G. Zheng, W. Liang, M. Hada, M. Ehara, K. Toyota, R. Fukuda, J. Hasegawa, M. Ishida, T. Nakajima, Y. Honda, O. Kitao, H. Nakai, T. Vreven, K. Throssell, J. A. Montgomery, Jr., J. E. Peralta, F. Ogliaro, M. J. Bearpark, J. J. Heyd, E. N. Brothers, K. N. Kudin, V. N. Staroverov, T. A. Keith, R. Kobayashi, J. Normand, K. Raghavachari, A. P. Rendell, J. C. Burant, S. S. Iyengar, J. Tomasi, M. Cossi, J. M. Millam, M. Klene, C. Adamo, R. Cammi, J. W. Ochterski, R. L. Martin, K. Morokuma, O.

---

Farkas, J. B. Foresman, D. J. Fox, Gaussian, Inc., Wallingford CT, 2016. Gaussian 16, Revision  
A.03, Gaussian, Inc., Wallingford CT, 2016.

